Published in final edited form as:
Magn Reson Med. 2012 July ; 68(1): 188–197. doi:10.1002/mrm.23226.

Contrast Enhancement in TOF cerebral angiography at 7 T using Saturation and MT pulses under SAR constraints: impact of VERSE and sparse pulses

Sebastian Schmitter[1], **Michael Bock**[2], **Sören Johst**[2], **Edward J. Auerbach**[1], **Kâmil Uğurbil**[1], and **Pierre-François Van de Moortele**[1]

[1]University of Minnesota, Center for Magnetic Resonance Research, Minneapolis, MN, United States

[2]German Cancer Research Center (DFKZ), Heidelberg, Germany

Abstract

Cerebral 3D time of flight (TOF) angiography significantly benefits from ultra high fields, mainly due to higher SNR and to longer T_1 relaxation time of static brain tissues, however, SAR significantly increases with B_0. Thus, additional RF pulses commonly used at lower field strengths to improve TOF contrast such as saturation of venous signal and improved background suppression by magnetization transfer typically cannot be used at higher fields. In this work we aimed at reducing SAR for each RF pulse category in a TOF sequence. We use the VERSE principle for the slab selective TOF excitation as well as the venous saturation RF pulses. Additionally, MT pulses are implemented by sparsely applying the pulses only during acquisition of the central k-space lines to limit their SAR contribution. Image quality, angiographic contrast and SAR reduction were investigated as a function of VERSE parameters and of the total number of MT pulses applied. Based on these results, a TOF protocol was generated that increases the angiographic contrast by more than 50% and reduces subcutaneous fat signal while keeping the resulting SAR within regulatory limits.

Keywords

time of flight; SAR; RF power; VERSE; MR angiography; ultra-high field MRI

Introduction

Time of flight (TOF) imaging is the most commonly used non-contrast enhanced MR angiography technique (1). In 3D TOF MR angiography a slab selective 3D steady state gradient echo sequence with a TR much shorter than the T_1 relaxation time of static tissue is used. A sufficiently large flip angle, typically 20°–40° (2), is applied to suppress MR signals of static tissue, whereas fully relaxed inflowing blood entering the excitation slab provides strong MR signal, resulting in a positive vessel contrast suitable for maximum intensity projection (MIP) reconstruction. TOF angiography has been shown to substantially benefit from high magnetic field of 7T, because of increased signal-to-noise ratio (SNR) (3) and longer T_1 relaxation times (4). However, for a given flip angle the specific absorption rate (SAR) of an RF pulse increases with B_0 (5), which may preclude the use at 7T of lower field protocol parameters.

Correspondence address: Sebastian Schmitter, PhD, Center for Magnetic Resonance Research (CMRR), University of Minnesota Medical School, 2021 6th St. SE, Minneapolis, MN 55455, USA, phone: 612-626-2001, fax: 612-626-2004, sschmitt@umn.edu.

Clinical TOF protocols at $B_0 \leq 3T$ already apply relatively high average RF power levels for several reasons. First, a short TR is used in combination with a relatively high flip angle. Second, the background signal suppression is routinely improved with Magnetization Transfer (MT) preparation pulses (2,6,7) that require high RF power. Third, to selectively image the intracranial arteries while reducing venous contributions, RF power-intensive spatial saturation pulses are used to saturate e.g. venous signal in the sagittal sinus. Because of these SAR constraints, TOF angiograms at 7T (8–13) were often obtained with suboptimal TR or excitation flip angle, and with venous saturation and MT pulses that were either absent, applied less frequently (9,12) or limited to narrow slabs of tissue using reduced bandwidth pulses (11), all tradeoffs that limit the capability of suppressing residual tissue background and venous blood signals.

The aim of this study was to implement SAR reduction strategies to use both venous saturation and MT pulses in TOF MRA protocols at 7T. For this purpose, the variable-rate selective excitation (VERSE) principle (14) was used to design excitation and saturation RF pulses, and a sparse excitation scheme was used to apply MT RF pulses (15). The impact of B_0 inhomogeneity and fat chemical shift on VERSE RF pulse excitation profiles at 7T was also investigated.

Methods

Experiments were performed on a whole body 7T system (Siemens Medical Solutions, Germany) equipped with either a whole body gradient or a head gradient coil, using a homebuilt 16-channel transceiver head coil similar to (16) powered with 16×1 kW RF amplifiers (Communication Power Corporation, USA). Healthy volunteers, who signed a consent form approved by the Institutional Review Board (University of Minnesota), were imaged in supine position. Using initial cerebral scout images the patient table was moved to position the Circle of Willis approximately at iso-center of the gradient coil.

VERSE RF pulse design

A VERSE RF pulse design algorithm, similar to the original proposal (14), was implemented in a TOF sequence using the manufacturer's programming tools (IDEA VB15). A standard RF pulse $b_1(n)$, available within the IDEA framework, was chosen as the starting point for the VERSE algorithm. The complex-valued RF pulse and the corresponding scalar gradient waveform $g(n)$ calculated by the sequence were defined for N samples of duration Δt (RF dwell time) with $n \in [1,2,\ldots,N]$. For simplicity, both $b_1(n)$ and $g(n)$ are assumed to be defined with same N and Δt values, thus with same duration $T = N \cdot \Delta t$. Gradient ramps *before* and *after* the RF pulse are not considered through the manuscript, thus the gradient amplitude during a standard RF pulse is constant with $g(n) = \hat{g}$. A VERSE RF pulse $b_1^V(n)$ and the corresponding VERSE gradient waveform $g^V(n)$ with slew rate $s^V(n)$ are then calculated based on $b_1(n)$ and $g(n)$, fulfilling four constraints:

$$T^V = T, \tag{1}$$

$$\left|g^V(n)\right| \leq g_{\max}, \tag{2}$$

$$\left|s^V(n)\right| \leq s_{\max}, \tag{3}$$

$$\left|b_1^V(n)\right| \leq b_{\max}. \quad (4)$$

Here T^V denotes the duration of the final VERSE pulse, $g_{\max}$, $s_{\max}$ and $b_{\max}$ denote the maximum gradient, slew rate and RF amplitude, respectively. $s_{\max}$ is set to a value of 100mT/m/ms and $b_{\max}$ is set to a fraction κ of the maximal RF amplitude of the initial pulse: $b_{\max} = \kappa \cdot \max[b_1(n)]$. The κ values utilized in our simulations and experiments were 100%, 50%, 33% and 25% for excitation RF pulses (κ_{EXC}), and 25% for saturation RF pulses (κ_{SAT}). The value of $g_{\max}$ is determined in order to keep the total RF pulse duration constant (Eq. 1). The VERSE RF pulse design essentially consists of stretching (shrinking) in time the segments of the initial RF pulse having high (low) amplitude, while RF and gradient amplitude are simultaneously decreased (increased) inversely to maintain the zeroth b_1 moment (i.e., the flip angle). To satisfy hardware constraints, RF and gradient waveforms are finally re-sampled on equidistant time raster with dwell times of $\Delta t_{RF}^V = 1\mu s$ for VERSE RF pulses and $\Delta t_G^V = 10\,\mu s$ for VERSE gradient waveforms. More details of the algorithm can be found in (17).

Initial and VERSE excitation RF pulses, both having a duration of 1536μs, are shown together with the corresponding gradient waveforms in Fig. 1 for κ_{EXC}= 100% (no VERSE), κ_{EXC}=50% and κ_{EXC}=25%. Under ideal conditions, the excitation pulses generate a rectangular shaped excitation profile. We refrained from using tilted optimized non-saturating excitation (TONE) RF pulses (18) to better estimate profile distortions resulting from ΔB_0. The same VERSE algorithm was applied to the venous saturation pulse targeting a 40mm-thick travelling slab, placed cranially to the excitation slab. The initial RF pulse shape was identical to Fig. 1 with a duration of 3584 μs for VERSE and non-VERSE RF pulse. Further details on RF pulse-related parameters are given in Table 1.

Excitation and saturation RF pulse profiles

Simulations—The impact of B_0 inhomogeneities on VERSE RF excitation profiles was investigated with numerical simulations of the Bloch equations. Transverse magnetizations after RF excitation were calculated using MATLAB (The MathWorks Inc., USA). In a first series of simulations, the value of κ_{EXC} was fixed to 25%, and the resonance frequency offset (Δf_{off}) was varied: −1kHz, 0Hz, +150Hz or +300Hz. (−1kHz approximates the fat chemical shift (~3.5ppm) at 7T). In a second series, Δf_{off} was set to 300Hz while the VERSE algorithm was applied with a κ_{EXC} value of 25%, 33% or 50%. All other simulation parameters are listed in Table 1.

Distortions of the resulting VERSE excitation profiles in the presence of a frequency offset were characterized by three parameters: average slope, slab center shift and side-lobe amplitude. The average slope of the slab profile was calculated from a linear fit to the slice profile using data points only within an interval of ±5mm around the slab center. Results are expressed as percentage of signal variation over the 10mm interval, relative to the signal amplitude at the slab center. The expected slab center position was determined based on the FWHM boundaries of the initial (ideal) profile, and the signal amplitude at these boundaries was used to calculate the slab center position of the distorted profile. The corresponding slab center shift was calculated relative to the ideal profile. The maximum side-lobe amplitude was normalized to the profile intensity at the center of the ideal slab. Numerical simulations were also performed to calculate longitudinal magnetization profiles when applying VERSE to saturation RF pulses with κ_{SAT}=25%.

Phantom and In-Vivo Experiments—Slab excitation profiles were measured for excitation RF pulses designed with κ_{EXC}=25%, using identical RF pulse parameters as in numerical simulations, with a modified version of the 3D TOF sequence allowing for imaging a larger FOV than the excitation slab along the slab direction. Prior to applying this TOF sequence, a multi-slice ΔB_0 map (dual gradient echo images, TE1/TE2=5.0/6.0ms) was acquired after second order B_0 shimming, and a 3D magnitude transmit B_1 (B_1+) map was obtained using the Actual Flip Angle (AFI) technique (19). For in-vitro experiments, excitation profiles were measured in a doped phantom (3.75g $NiSO_4$ + 5g NaCl per 1000g H_20; measured T_1=80ms) with imaging parameters listed in Table 2. The imaging FOV along the slab direction was set to 72mm, i.e. three times the nominal 24mm excitation thickness of the axial slab, to visualize profile side-lobes and to avoid aliasing. To remove spatial transmit and receive variations of the RF coil from the profile, an additional 3D acquisition was obtained using identical imaging parameters except for a non-selective RF excitation, and a large FOV of 240mm in slab direction to avoid aliasing. Saturation effects were reduced by using a phantom with a short T_1 together with a relatively small flip angle (20°) and a TR≈T_1 (80ms). The total acquisition time for the 3D dataset was 41min. The difference between measured and simulated profiles was quantified by root mean square error (RMSE).

In-vivo excitation profiles were obtained in the human brain. To reduce the acquisition time while limiting the impact of long T_1 relaxation times (about 1220ms/2132ms/4200ms in gray-matter/white-matter/CSF at 7T (4)), acquisitions were performed at a lower spatial resolution (cf. Table 2) and with a smaller flip angle (8°). For further analysis of profile distortions resulting from ΔB_0 inhomogeneities, two 3-by-3 pixel ROIs were defined: one in the frontal lobe, above the nasal cavity where ΔB_0 is typically ~1ppm, the other in the center of the brain, where the transmitter frequency was calibrated. Average profiles along the slab direction were calculated for both ROIs.

TOF acquisition

3D TOF data sets were acquired as multiple, partially overlapping thin slabs merged during image post-processing (20). Prior to TOF measurements, ΔB_0 and B_1+ maps were acquired and the transmitter frequency was set to the Larmor frequency in the center of the brain, based on the measured ΔB_0 maps. The transmitter voltage was calibrated for the nominal flip angle at the Circle of Willis. Different TOF acquisitions, described below, were performed to investigate the impact of using VERSE excitation pulses, of applying VERSE venous saturation pulses and of including sparse MT pulses. Based on these results, a trade-off was determined to acquire high contrast, multi-slab TOF angiograms within acceptable SAR limits.

Impact of κ_{EXC} in the presence of ΔB_0—To study in-vivo the impact of κ_{EXC} on the signal at slab overlaps, TOF datasets were acquired using three different κ_{EXC} values for VERSE excitation RF pulse design: 100% (no VERSE), 50% and 25%. Neither venous saturation nor MT was enabled for this acquisition. Because errors in the excitation slab profile can especially alter image quality at slab junctions, the inter-slab overlap, usually set to 25% (default value) to ensure smooth transitions through slabs, was reduced to 15% to better identify profile errors close to slab edges. Imaging parameters for this acquisition were: TR/TE=27ms/2.7ms, α=20, FOV=220×172×65mm^3, 3 slabs of 24mm thickness, 0.6mm isotropic voxels.

Impact of VERSE saturation pulses—Four different TOF acquisitions were compared to investigate the impact of applying VERSE on saturation pulses: *i*) TOF sequence with initial excitation pulses (no VERSE) and without venous saturation pulses, *ii*) VERSE

applied on excitation pulses (κ_{EXC}=50%) but no saturation pulses were used, *iii*) VERSE applied on excitation and saturation pulses (κ_{EXC}=50%, κ_{SAT}=25%), *iv*) same acquisition as *iii* but with reversed polarity of saturation slab selection gradient (together with opposite sign of transmitter frequency offset). The latter acquisition was performed to investigate the effects of the saturation RF pulses on fat signal within the imaging slab. Other imaging parameters are summarized in the rightmost column of Table 2 except that only one slab was acquired to reduce the acquisition time. In five subjects the venous signal suppression was quantified by calculating a venous vessel-to-background-ratio (vVBR), i.e. the ratio of the average signal in the sagittal sinus and the average signal from static background tissue surrounding the sinus.

Impact of MT pulses—MT pulses were applied sparsely, i.e. only on N_{MT} central k-space lines out of N_{TOT} total lines. In this study the ratio N_{MT}/N_{TOT} was increased from 0% to 36% and the highest N_{MT} value was determined based on the maximum acceptable SAR. No venous saturation was applied; imaging parameters were identical to Table 2 (rightmost column) but with one slab. To optimize the TOF contrast, an arterial vessel-to-background ratio (aVBR) was determined as a function of N_{MT}/N_{TOT} by dividing the average signal in the basilar artery close to the Circle of Willis by the average signal from the surrounding background tissue. For comparison, aVBR was also calculated in other protocols, either with VERSE saturation pulses enabled (κ_{SAT}=25%), or without saturation *and* without MT pulses.

TOF Tradeoff—Based on the results of the previous measurements a TOF protocol was defined, using the acquisition parameters listed in Table 2 (rightmost column), and including VERSE excitation, VERSE saturation and sparse MT pulses. For contrast comparison, this protocol was acquired with two different settings: *i*) without VERSE, without saturation pulses and without MT pulses, *ii*) with VERSE excitation/saturation pulses and with sparse MT pulses. In the latter case N_{MT}/N_{TOT} was set to 10% using 17 and 38 k-space lines in slab selection (SL) and phase encoding (PE) direction. The acquisition time for this high resolution protocol was 14min 36s. All SAR values are given in units of the maximum acceptable limit (SAR_{MAX}) as provided by the system software.

Results

Excitation and saturation VERSE RF pulse profiles

In general, with decreasing κ_{EXC} or increasing ΔB_0 VERSE excitation profiles show an increased average slope, slab center shift and side-lobe amplitude (Fig. 2a+b). With κ_{EXC}=25%, a 300Hz frequency offset generates an excitation profile with a slope of 45.5%, a side-lobe amplitude of 21.9% and a slab shift of 11.1%. By comparison, without VERSE (κ_{EXC}=100%) there is no slope trend, the side-lobe amplitude is 2.3%, and a 4.9% shift of the slab center is seen (Fig. 2a). The excitation profile for fat signal (−1kHz offset) shows a strongly distorted, asymmetric shape with the maximum signal peak shifted by −13.7mm from the original slice center (Fig. 2b).

Similar distortions are observed for the longitudinal magnetization profile of a venous saturation RF pulse with a target slab thickness of 40mm, as shown in Fig. 2c for κ_{SAT}=25%. As expected, both the slope and the center slab shift vary as a function of the resonance offset. Note that the gradient polarity determines the relative shift direction of the saturation profile for fat protons, i.e., either *towards* or *away from* the TOF imaging slab. This shift can be used to intentionally overlap the fat saturation of the venous saturation pulse with the TOF imaging slab to suppress fat in the final TOF images (21). This is

illustrated in Fig. 2c where the fat saturation is strongest at −59mm from the center of the venous saturation slab.

Experimental and simulation profiles for VERSE RF pulses were in good agreement, as illustrated in Fig. 2d where measured (in a phantom) and simulated profiles are shown for κ_{EXC}=25% in the absence of significant ΔB_0 (<0.1ppm). An RMSE between simulation and experiment of 0.7% was found for the total acquisition window, and of 0.5% within the slice. The same reference voltage was used for all subjects, with a mean flip angle value measured within the Circle of Willis of 24.1°±1.4° (minimum 22.7°, maximum 26.2°) for a nominal flip angle of 24°. SAR generated by excitation and saturation pulses is dependent on κ_{EXC} and κ_{SAT}: applying the VERSE principle neither to saturation nor to excitation would yield SAR values at 119% of SAR_{MAX} for a protocol given in Table 2 (TOF protocol). By contrast, using VERSE with κ_{EXC}=50% and κ_{SAT}=25% (as used in our TOF tradeoff protocol), results in 49% of SAR_{MAX}. In-vivo slice profiles are demonstrated in Fig. 3 for two ROIs: one positioned in the frontal lobe where strong off-resonances between 245Hz and 48Hz occur, one positioned close to the center of the brain, where the off-resonance is between −9.0Hz and −2.7Hz. For the ROI in the frontal lobe with large offset frequencies the slice profiles agree qualitatively with the simulations and the phantom experiments even though a highly heterogeneous ΔB_0 distribution is present over the slab. The impact of ΔB_0 on multi-slab TOF images acquired with VERSE pulses is especially noticeable in the sagittal MIP images at the junctions between adjacent slabs (Fig. 4). Note that a reduced slab overlap was used intentionally to visualize the slab boundaries, which resulted in dark stripes between adjacent slabs (‘venetian blind’ artifact). Slab edges were most distorted at the lowest κ_{EXC} value (25%) in regions with high ΔB_0 (frontal lobe above the nasal cavity, white arrows). This dependence on κ_{EXC} is further emphasized in the line plots obtained from the source images at the same location (dashed line): noticeable distortions are observed with κ_{EXC}=25%, whereas no significant alterations are seen with κ_{EXC}=50% compared to κ_{EXC}=100%.

Based on these findings, in all subsequent TOF acquisitions a value of κ_{EXC}=50% was chosen. For venous saturation pulses, however, κ_{SAT} was set to 25% because venous slab profile accuracy is not as critical as TOF slab profile accuracy. Additionally, the spatially shifted fat suppression profile generated by VERSE saturation may overlap with the excitation slab, resulting in improved MIP image quality, and the large SAR reduction allows for applying sparse MT pulses, which further contribute to a better image quality.

Contrast enhancement within SAR limits

Figure 5 compares 3D TOF datasets obtained with a) no VERSE excitation and no saturation, b) with κ_{EXC}=50% and no saturation, c) with κ_{EXC}=50% and κ_{SAT}=25%, d) with same parameters as in *c* but with reversed polarity of the saturation slab selection gradient (and transmitter frequency offset). The comparison of Fig. 5a with Fig. 5b shows that VERSE excitation does not reduce the image quality: the mean aVBR of the 5 subjects was 6.07±0.53 for κ_{EXC}=50% and 6.26±0.54 for κ_{EXC}=100%. At the same time, the corresponding relative SAR reduction to 58%, even though relatively limited, provided more flexibility for further usage of saturation (or MT) pulses.

VERSE saturation pulses effectively suppressed venous signals for example in the sagittal sinus (Figs. 5c and 5d). Here, the mean vVBR, determined in 5 subjects, was significantly reduced from 3.72±0.17 without saturation to 0.29±0.03 with κ_{SAT}=25%. Furthermore, fat signals were strongly reduced within the imaging slab when the correct gradient polarity was chosen (Fig. 5d), consistent with the spatial shift observed in the fat saturation profiles simulated with VERSE saturation pulses (Fig. 2c). At the slab center the fat signal reduction was larger than 80%, whereas no fat suppression was observed with opposite gradient

polarity (Fig. 5c). Note that in the latter case signals from brain tissues (instead of signals from fat) in areas of large ΔB_0 variations were partially saturated, as for example in the inferior part of the frontal lobe (Fig. 5c). In addition to the saturation of venous blood and fat, a visible reduction in background signal was obtained improving the contrast from aVBR = 6.07±0.53 without saturation to 7.59±0.73 with VERSE saturation.

On coronal and sagittal views of 3D TOF datasets, signal aliasing in slab direction was seen with VERSE excitation pulses and without saturation pulses (Fig. 5b, white arrows), identified as fat signals excited outside the imaging slab. The chemical shift between water and fat is only 2.2mm when κ_{EXC}=100% is used, thus with 25% oversampling (8mm) in the slab direction no aliasing artifact is seen without VERSE excitation (Fig. 5a). Interestingly, the aliased fat signal was strongly reduced in Fig. 5d due to the shifted fat saturation slab with VERSE saturation. As demonstrated in Fig. 6 and Table 3 additional gains in aVBR can be obtained with sparse MT pulses. Figure 6 shows aVBR (circles) as a function of N_{MT}/N_{TOT} with κ_{EXC}=50% and without saturation pulse. It can be seen that aVBR first increases from about 6 to 7.25 in the range of 0% to 10%, and then only gradually for N_{MT}/N_{TOT}>10%. Simultaneously, the relative SAR of the MT pulses (dashed line) increases linearly with N_{MT}/N_{TOT}, theoretically reaching up to 204% of SAR_{MAX} for N_{MT}/N_{TOT}=100%. Therefore, a value of N_{MT}/N_{TOT}=10% was used in all further in-vivo measurements with MT. Table 3 (rightmost column) summarizes the mean aVBR over all 5 subjects for different combinations of excitation, saturation and MT pulses. The use of VERSE excitation pulses alone does not significantly alter aVBR, but with VERSE saturation or sparse MT aVBR increases by approximately 19% or 21%, respectively. With both saturation and sparse MT, aVBR reaches values of 9.40±1.03, an increase of about 50% compared to the initial TOF settings.

The overall improvement when VERSE excitation, VERSE saturation and MT are simultaneously applied is seen in the MIP images in Fig. 7. Background and fat signals are reduced, especially in the brain periphery, smaller vessels become visible, and bright venous signal is effectively suppressed. This combination of contrast enhancement would not have been possible without the implementation of substantial SAR reduction strategies, as can be seen in Table 3, showing that using saturation and MT pulses with the initial TOF sequence (no VERSE) would yield 319% of SAR_{MAX}.

Discussion

Increasing spatial resolution in cerebral MRA can have a significant clinical impact, as it allows detecting lesions or anomalies of brain vessels of very small diameter. This provides a strong rationale to investigate cerebral TOF at ultra high field where gains in SNR and longer tissue T_1 relaxation times may help improving spatial resolution and vessel depiction. However, due to SAR limitations at higher field, sequence components that substantially improve TOF contrast and are commonly utilized at 1.5T and 3T have been omitted, or utilized at a suboptimal level, in TOF studies reported so far at 7T (8–13). Our results indicate, that indeed such contrast enhancement modules in their native form would generate about 319% of SAR_{MAX} in our 7T TOF protocol. In this study, we aimed at reducing SAR for each RF pulse category in a TOF pulse sequence that includes, as in lower field protocols, venous saturation and MT. Most of the components used in this work to increase TOF contrast have been individually investigated at lower field (6,7,14,15,21,22). However, to our knowledge, is has not been reported that VERSE applied on single slab selective RF saturation pulses in TOF can be used to limit SAR while providing simultaneously venous saturation above the imaging slab, fat saturation within the imaging slab and MT for enhanced background suppression.

For excitation and saturation pulses, SAR was reduced by applying the VERSE principle. It was important to investigate at 7T the impact of ΔB_0 on the slice profile quality. Based on simulations and experiments, excitation and saturation profile distortions induced by VERSE in the presence of off-resonance spins were characterized by a global spatial shift, larger side-lobes and overall ramp shaped profiles. All these effects were inversely dependent on the maximum allowed B_1 amplitude, controlled by the factor κ_{EXC} (or κ_{SAT}), which determines how aggressively the VERSE algorithm is applied to reduce SAR. Severe distortions of the excitation profile may cause signal drops at junctions of overlapping slabs, as seen in Fig. 4, and may reduce signal homogeneity in vessels traversing the slab, depending on blood velocity. In addition, side-lobes may cause aliasing artifacts. For TOF MRA applications, excitation profiles were satisfactory as long as VERSE excitation pulses were designed with $\kappa_{EXC} \geq 50\%$.

In clinical applications, TONE pulses with ramp shaped excitation profiles are often used to reduce arterial blood saturation through the imaging slab. In this work however, only RF pulses with rectangular excitation profile were used to obtain a better estimation of excitation profile alterations when using VERSE pulses. Similar profile alterations however have been reported with VERSE TONE RF pulses at 7T (23).

With VERSE, saturation pulse side-lobes resulting from off-resonance offsets impair neither venous saturation nor image quality as long as they do not reach into the imaging slab. Ramps and spatial shifts may in principle alter the effectiveness of the venous saturation, but this effect was found to be moderate as long as a sufficiently large mean saturation flip angle was maintained. Thus, VERSE saturation pulses designed with $\kappa_{SAT} \geq 25\%$ provided satisfactory quality.

From an SAR level perspective, applying VERSE on saturation pulses resulted in larger total SAR reduction than on excitation pulses, as expected, given the typically high RF power demand for saturation pulses. This, together with the sensitivity of the VERSE excitation profile to ΔB_0, could be seen as a reason to apply VERSE only to saturation pulses and not to excitation pulses. However, there are situations where the additional SAR reduction from the VERSE excitation pulses can provide an extra degree of freedom. For example, it has been shown that B_1 shimming can improve TOF contrast homogeneity (24). Homogeneous B_1 shimming solutions, however, tend to result in higher RF power, thus higher SAR, for a given flip angle.

Note that the TOF protocols were limited by SAR, not by RF amplifiers. The maximum total RF peak power was always below 400W; it is thus anticipated that with a single transmit channel head coil, a 8kW amplifier would be sufficient, even considering losses on the transmit RF path. Regarding the saturation pulses, SAR reduction could in principle be obtained by lowering the saturation flip angle, thus the RF voltage. For example a saturation flip angle of 45° instead of 90° may provide sufficient venous blood suppression. However, at 7T B_1+ profiles in the head typically present large spatial heterogeneities. In this study, flip angles through the brain could vary as much as between 12° and 90° for a nominal value of 60°. Reducing the overall saturation RF power in this case may not provide satisfactory saturation in locations of low B_1+ magnitude. (Note that a somewhat weaker fat suppression observed in the frontal part of the head is possibly the result of a weaker local B1+).

Another, well known alternative to reduce SAR consists of prolonging RF pulses to the cost of increasing minimum TR and TE. In this work, however, we demonstrated that even under the more demanding constraint of constant minimum TR, TOF contrast enhancement can successfully be obtained at 7T without reaching SAR limits. We found that the shortest possible TR with saturation and MT pulses (TR=33ms), together with a flip angle of 24°,

provided a satisfactory tradeoff between TOF contrast and acquisition time. To reduce SAR with longer pulses at a similar spatial fat chemical shift, saturation pulses without VERSE would require a 3.1 times longer duration.

Because of the large fat chemical shift at 7T, the profile of VERSE excitation pulse also shows a spatial shift for fat protons along the slab direction (Fig. 2b). This causes the aliasing artifacts from fat in Fig. 5, despite the 25% image slab oversampling (8mm) along the slab direction. Cerebral TOF MIP angiograms are not directly impaired by these artifacts, because aliased subcutaneous fat signals are still restricted outside brain tissues. Furthermore, this fat artifact was suppressed by up to 90% by the shifted fat profile of VERSE saturation pulse with correct slab selective gradient polarity. Additional control on the location of maximum fat signal suppression is obtained by adjusting the distance between imaging and saturation slabs. In this work we used an inter-slab distance of 10mm, resulting in fat suppression peak localized at 5mm below the imaging slab, a combination that provided strong attenuation of fat aliasing artifacts while preserving efficient vein suppression. Finally, the fat saturation profile can also be tailored by adjusting saturation slab thickness and/or κ_{SAT}.

As seen in Fig. 5, venous saturation RF pulses do not only reduce signals from venous blood and aliased fat, they also significantly enhance the arterial contrast due to an increased background suppression that results from MT properties of saturation pulses. This effect has been reported by Miyazaki (22) with a slab selective MT pulse reducing background signals without affecting inflowing arterial blood spins. In our experiments the ratio of background signal *with* saturation to background signal *without* saturation amounted to 0.778±0.074, whereas the corresponding ratio of signal intensity within the arterial vessel remained unchanged.

Besides the magnetization transfer component of saturation pulses, the addition of sparse MT pulses significantly increased the angiographic contrast, as previously reported at lower field (15,25). However, even after the large SAR reduction obtained when applying VERSE on excitation and saturation pulses, MT pulses could only be applied to a small fraction of k-space without exceeding SAR_{MAX}. As shown in Fig. 6, the main contrast improvement was obtained with MT applied to 10% of the k-space lines (a level at which SAR increases about 20%). Increasing the fraction beyond 10% only modestly improved the angiographic contrast, at the cost of substantial increase in SAR. Interestingly, the contrast improvement from sparse MT pulses and from the MT component of the saturation pulses appear to add up, as seen in Table 3, resulting in 50% higher angiographic contrast when using *both* VERSE saturation and sparse MT pulses compared to the initial TOF sequence. Corresponding enhanced visibility of smaller vessels can be visually appreciated in Fig. 7.

In summary, enabling VERSE for excitation (κ_{EXC}=50%) and saturation pulses (κ_{SAT}=25%) reduced SAR by a factor of more than 2.3 in a 3-slab TOF 7T protocol at $0.49\times0.49\times0.50mm^3$ resolution. Simultaneously the artery-to-background contrast ratio was improved and signals from veins and subcutaneous fat were attenuated. The SAR reduction allowed for implementing sparse MT pulses (10% of k-space lines) for additional background suppression, with the total SAR amounting to 69% of SAR_{MAX}; this number preserves some flexibility for clinical situations where higher SAR levels may be reached for a given protocol (e.g. larger RF coil load).

Acknowledgments

This work was funded by: German Research Foundation, grant number DFG SCHM 2677/1-1; National Institutes of Health, grant numbers P41 RR008079, P30 NS057091, R01 EB000331; Keck Foundation.

References

1. Miyazaki M, Lee VS. Nonenhanced MR angiography. Radiology. 2008; 248(1):20–43. [PubMed: 18566168]
2. Bernstein, MA.; King, KF.; Zhou, XJ. Handbook of MRI Pulse Sequences. Elsevier Academic Press; 2004.
3. Ugurbil K, Adriany G, Andersen P, Chen W, Garwood M, Gruetter R, Henry PG, Kim SG, Lieu H, Tkac I, Vaughan T, Van De Moortele PF, Yacoub E, Zhu XH. Ultrahigh field magnetic resonance imaging and spectroscopy. Magn Reson Imaging. 2003; 21(10):1263–1281. [PubMed: 14725934]
4. Rooney WD, Johnson G, Li X, Cohen ER, Kim SG, Ugurbil K, Springer CS Jr. Magnetic field and tissue dependencies of human brain longitudinal 1H2O relaxation in vivo. Magn Reson Med. 2007; 57(2):308–318. [PubMed: 17260370]
5. Vaughan JT, Garwood M, Collins CM, Liu W, DelaBarre L, Adriany G, Andersen P, Merkle H, Goebel R, Smith MB, Ugurbil K. 7T vs. 4T: RF power, homogeneity, and signal-to-noise comparison in head images. Magn Reson Med. 2001; 46(1):24–30. [PubMed: 11443707]
6. Lin W, Tkach JA, Haacke EM, Masaryk TJ. Intracranial MR angiography: application of magnetization transfer contrast and fat saturation to short gradient-echo, velocity-compensated sequences. Radiology. 1993; 186(3):753–761. [PubMed: 8430184]
7. Edelman RR, Ahn SS, Chien D, Li W, Goldmann A, Mantello M, Kramer J, Kleefield J. Improved time-of-flight MR angiography of the brain with magnetization transfer contrast. Radiology. 1992; 184(2):395–399. [PubMed: 1620835]
8. Kang CK, Park CW, Han JY, Kim SH, Park CA, Kim KN, Hong SM, Kim YB, Lee KH, Cho ZH. Imaging and analysis of lenticulostriate arteries using 7.0-Tesla magnetic resonance angiography. Magn Reson Med. 2009; 61(1):136–144. [PubMed: 19097221]
9. Conijn MM, Hendrikse J, Zwanenburg JJ, Takahara T, Geerlings MI, Mali WP, Luijten PR. Perforating arteries originating from the posterior communicating artery: a 7.0-Tesla MRI study. Eur Radiol. 2009; 19(12):2986–2992. [PubMed: 19533146]
10. Heverhagen JT, Bourekas E, Sammet S, Knopp MV, Schmalbrock P. Time-of-flight magnetic resonance angiography at 7 Tesla. Invest Radiol. 2008; 43(8):568–573. [PubMed: 18648256]
11. Maderwald S, Ladd SC, Gizewski ER, Kraff O, Theysohn JM, Wicklow K, Moenninghoff C, Wanke I, Ladd ME, Quick HH. To TOF or not to TOF: strategies for non-contrast-enhanced intracranial MRA at 7 T. MAGMA. 2008; 21(1–2):159–167. [PubMed: 18175158]
12. Zwanenburg JJ, Hendrikse J, Takahara T, Visser F, Luijten PR. MR angiography of the cerebral perforating arteries with magnetization prepared anatomical reference at 7 T: comparison with time-of-flight. J Magn Reson Imaging. 2008; 28(6):1519–1526. [PubMed: 19025959]
13. von Morze C, Xu D, Purcell DD, Hess CP, Mukherjee P, Saloner D, Kelley DA, Vigneron DB. Intracranial time-of-flight MR angiography at 7T with comparison to 3T. J Magn Reson Imaging. 2007; 26(4):900–904. [PubMed: 17896360]
14. Conolly S, Nishimura DG, Macovski A, Glover G. Variable-rate selective excitation. J Magn Reson. 1988; 78:440–477.
15. Parker DL, Buswell HR, Goodrich KC, Alexander AL, Keck N, Tsuruda JS. The application of magnetization transfer to MR angiography with reduced total power. Magn Reson Med. 1995; 34(2):283–286. [PubMed: 7476089]
16. Adriany G, Van de Moortele PF, Ritter J, Moeller S, Auerbach EJ, Akgun C, Snyder CJ, Vaughan T, Ugurbil K. A geometrically adjustable 16-channel transmit/receive transmission line array for improved RF efficiency and parallel imaging performance at 7 Tesla. Magn Reson Med. 2008; 59(3):590–597. [PubMed: 18219635]
17. Schmitter S, Bock M. Acoustic noise-optimized VERSE pulses. Magn Reson Med. 2010; 64(5): 1446–1452. [PubMed: 20597118]
18. Atkinson D, Brant-Zawadzki M, Gillan G, Purdy D, Laub G. Improved MR angiography: magnetization transfer suppression with variable flip angle excitation and increased resolution. Radiology. 1994; 190(3):890–894. [PubMed: 8115646]

19. Yarnykh VL. Actual flip-angle imaging in the pulsed steady state: a method for rapid three-dimensional mapping of the transmitted radiofrequency field. Magn Reson Med. 2007; 57(1):192–200. [PubMed: 17191242]

20. Parker DL, Yuan C, Blatter DD. MR angiography by multiple thin slab 3D acquisition. Magn Reson Med. 1991; 17(2):434–451. [PubMed: 2062215]

21. Doyle M, Matsuda T, Pohost GM. SLIP, a lipid suppression technique to improve image contrast in inflow angiography. Magn Reson Med. 1991; 21(1):71–81. [PubMed: 1943680]

22. Miyazaki M, Kojima F, Ichinose N, Onozato Y, Igarashi H. A novel saturation transfer contrast method for 3D time-of-flight magnetic resonance angiography: a slice-selective off-resonance sinc pulse (SORS) technique. Magn Reson Med. 1994; 32(1):52–59. [PubMed: 8084237]

23. Schmitter, S.; Johst, S.; Bock, M.; Ugurbil, K.; Van de Moortele, PF. Implementing VERSE for Time of Flight RF Pulses at 7Tesla: Methodological Considerations. Proceedings of the 18th Annual Meeting of ISMRM; Stockholm, Sweeden. 2010. (Abstract 4424)

24. Schmitter, S.; Auerbach, EJ.; Adriany, G.; Ugurbil, K.; Van de Moortele, PF. Improving TOF angiography contrast homogeneity with B1+ shimming at 7 Tesla: benefits and challenges. Proceedings of the 19th Annual Meeting of ISMRM; Montral, Canada. 2011. (Abstract 1287)

25. Lin C, Bernstein MA, Gibbs GF, Huston J 3rd. Reduction of RF power for magnetization transfer with optimized application of RF pulses in k-space. Magn Reson Med. 2003; 50(1):114–121. [PubMed: 12815686]

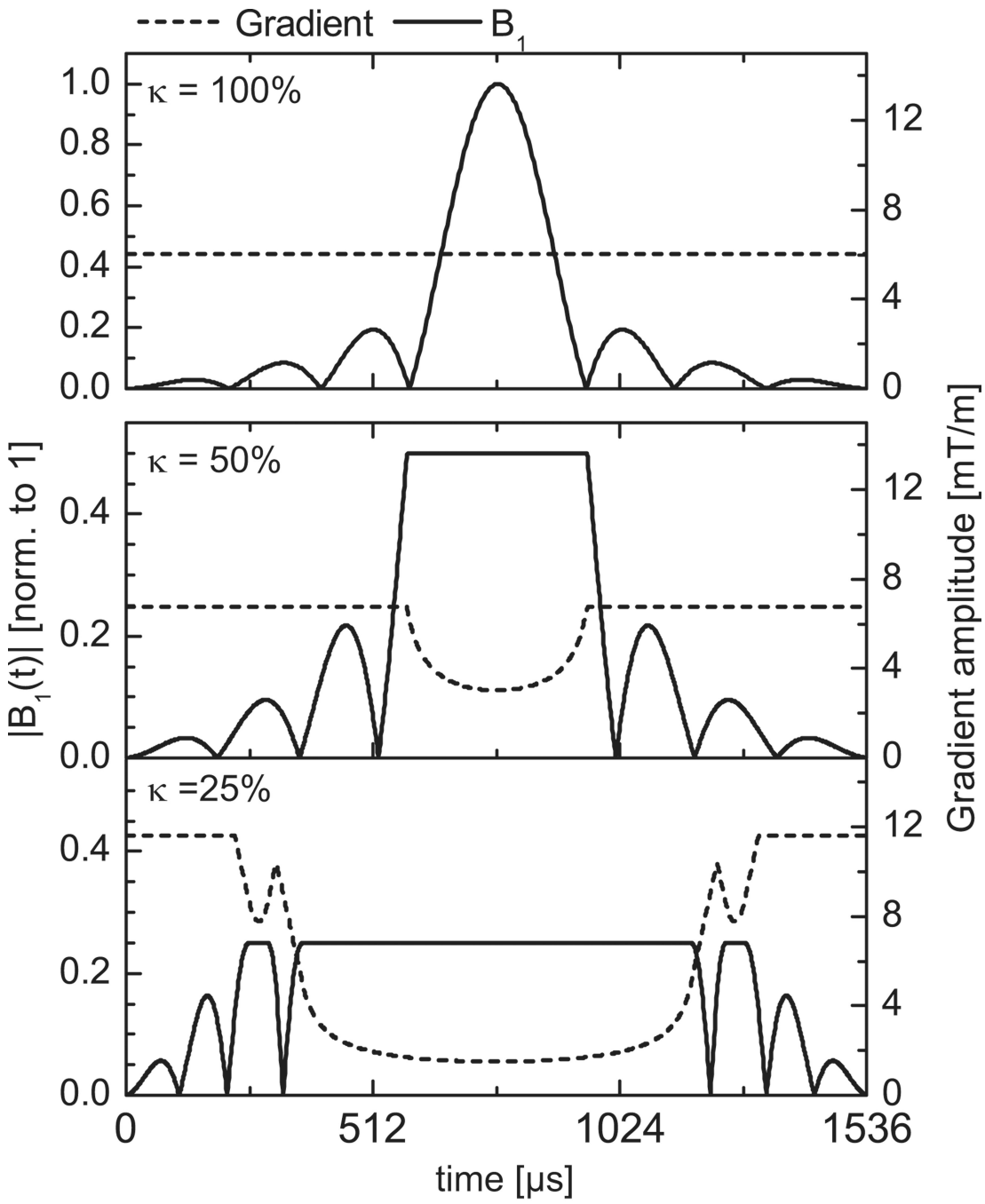

Figure 1.

Top: Initial gradient waveform and RF excitation pulse shape. *Middle and Bottom*: Gradient waveforms and RF excitation pulse shapes after applying VERSE with maximum RF amplitude reduced to κ_{EXC}=50% (middle) or κ_{EXC}=25% (bottom) of the initial RF pulse maximum amplitude. Note that the left vertical scale was reduced from [0–1] (top) to [0–0.5] (middle and bottom) for better visualization.

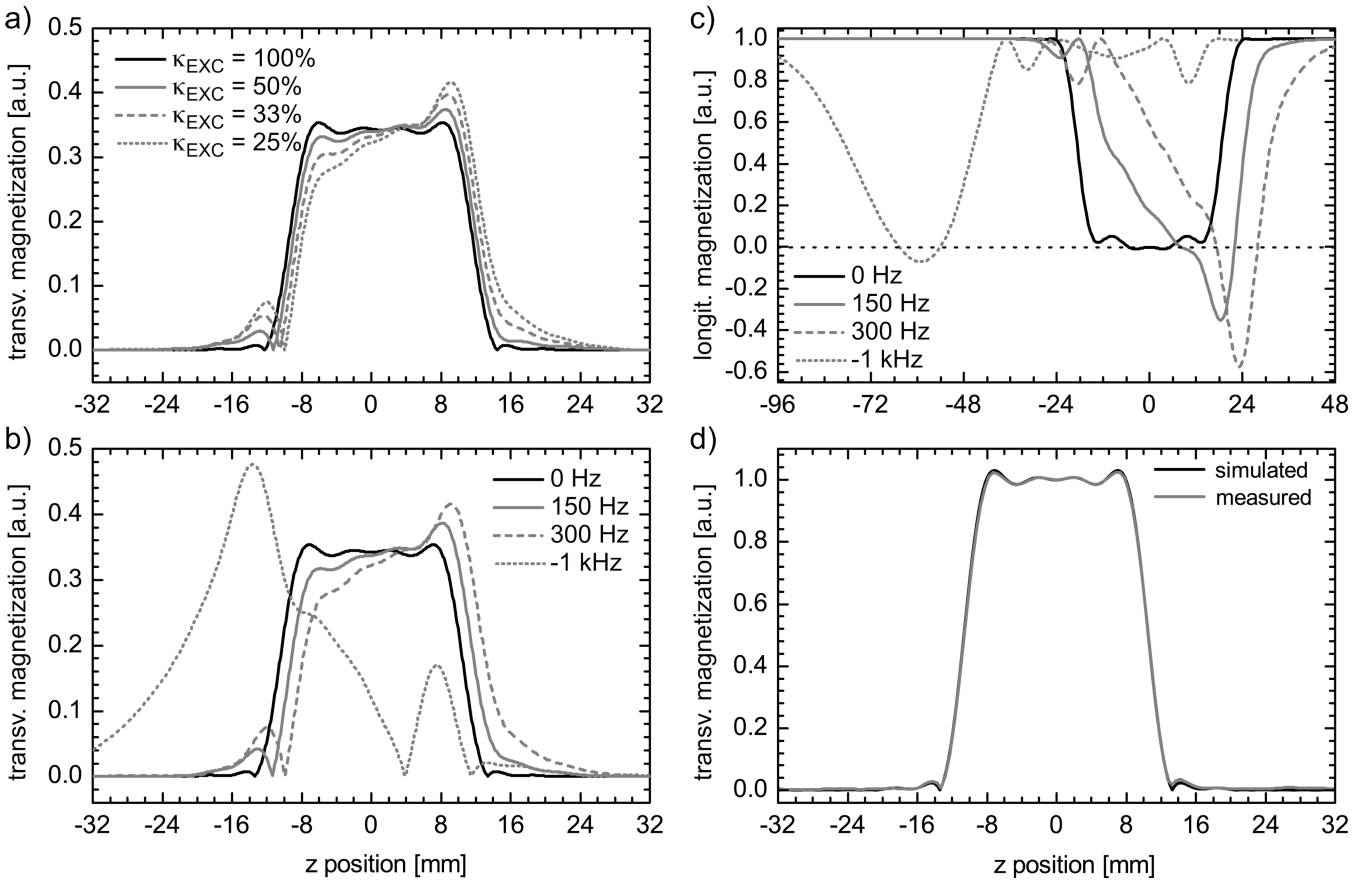

Figure 2.

a) Simulated excitation profiles, in presence of a fixed frequency offset of 300 Hz, obtained for the initial RF pulse and for VERSE pulses designed with different values of RF amplitude threshold κ_{EXC}. b) Simulated slice profile for VERSE pulses, designed with a fixed RF amplitude threshold κ_{EXC} of 25%, in the presence of different frequency offsets. The offset of −1 kHz was used to simulate fat excitation profile (~3.5 ppm chemical shift at 7 T). c) Simulated saturation profile showing the longitudinal magnetization for κ_{SAT}=25% and different frequency offsets. d) Measured excitation profile in a phantom with κ_{EXC}=25% and corresponding simulated profile without frequency offset including TR and T_1 of the phantom measurement.

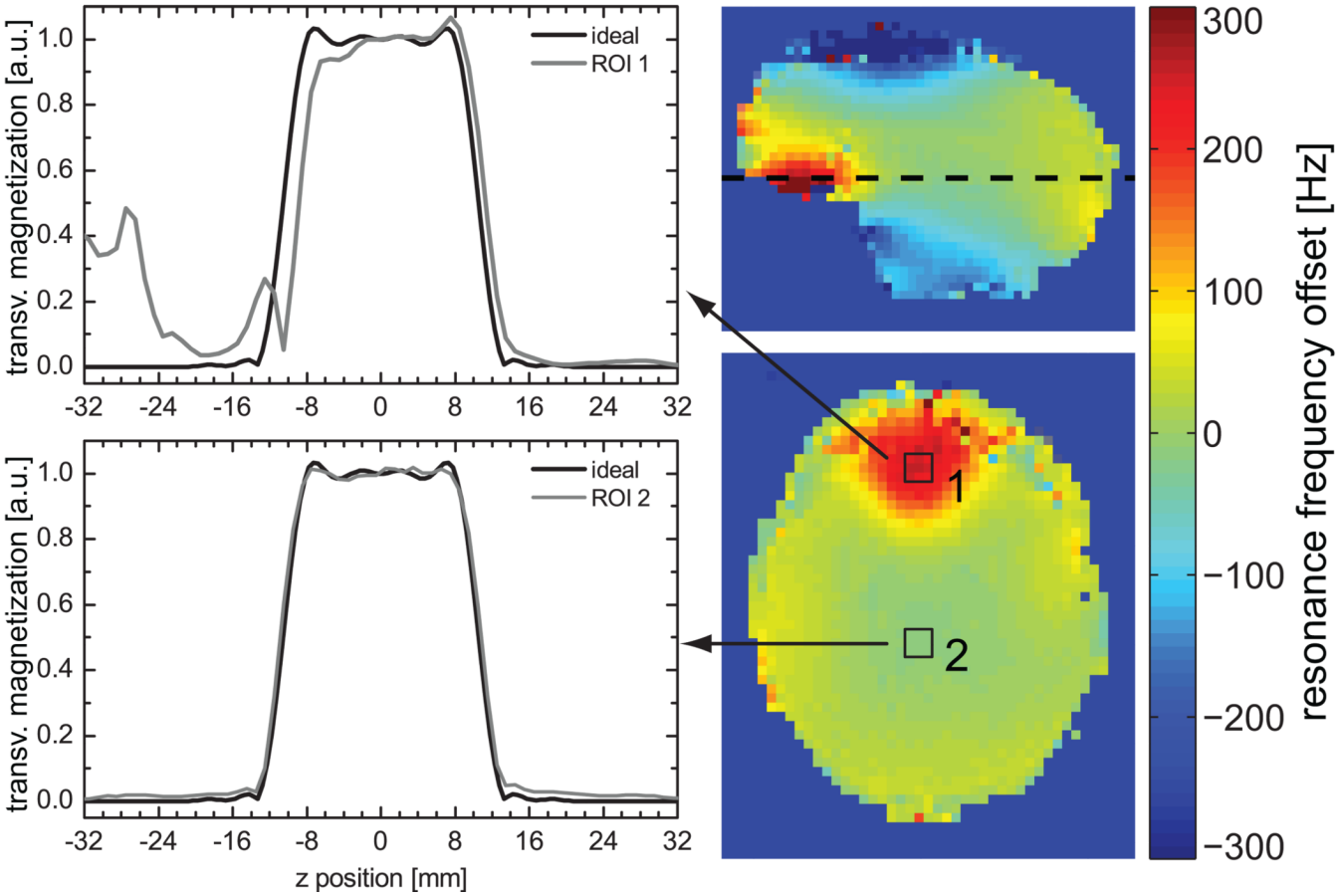

Figure 3.

Left: In-vivo slice profiles for an ROI located in an area with large ΔB_0 distortion (ROI 1) and for an ROI located in an area with no significant ΔB_0 variation (ROI 2). *Right*: ΔB_0 field maps in sagittal (top) and axial (bottom) views. The black squares indicate the location of the two ROIs. The horizontal dashed line on the sagittal view signals the location of the axial map that coincides with the lower edge of the excited slab (i.e. abscissa position ~= −12 mm on left plots).

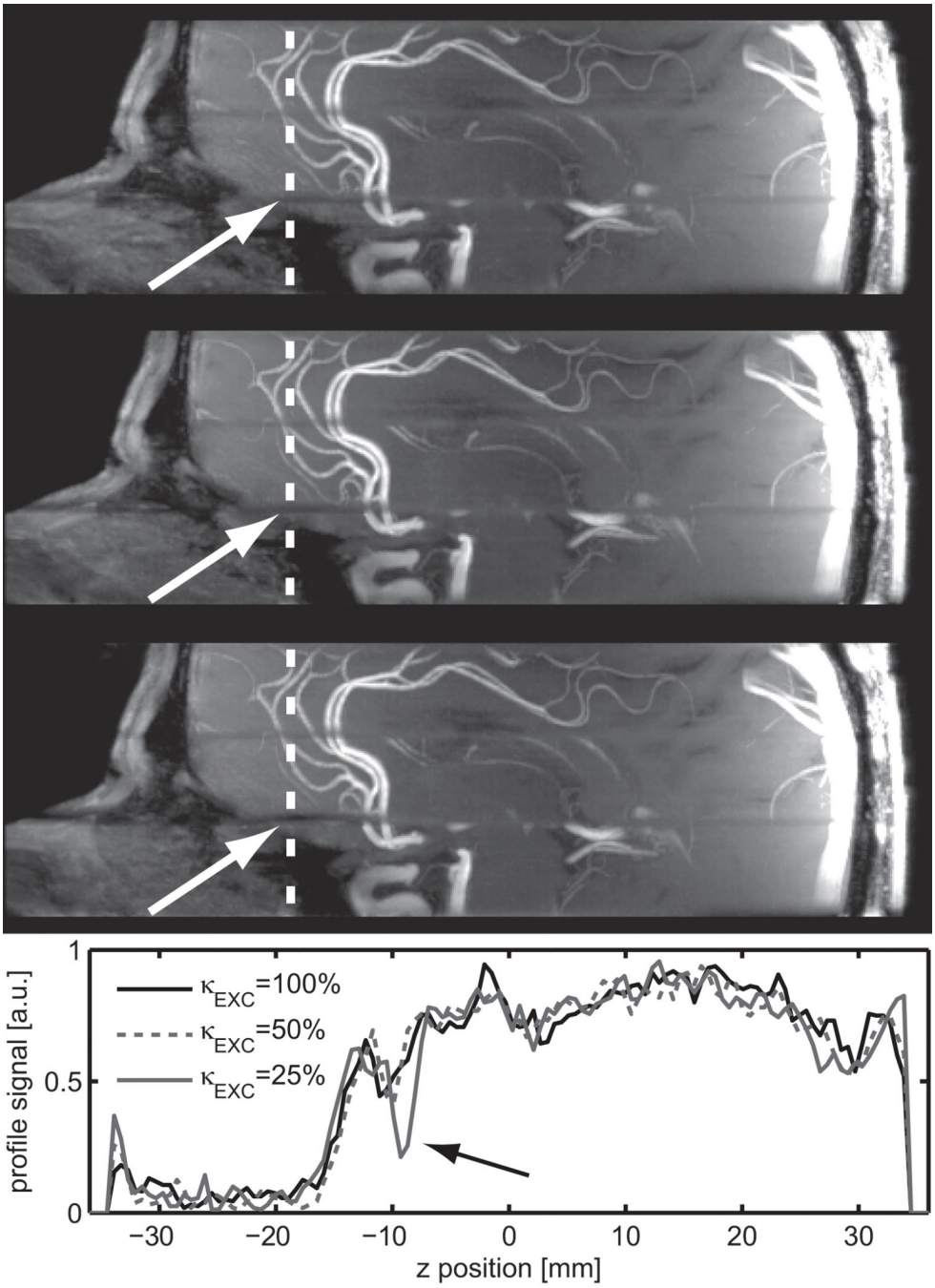

Figure 4.

Sagittal thin MIP images (15 mm thickness) generated from a TOF acquisition using a slab overlap reduced to 15%. The top image was acquired without using VERSE, the middle and bottom image were acquired with VERSE (κ_{EXC}=50% middle, κ_{EXC}=25% bottom). The white arrows indicate areas of large ΔB_0 distortion. The bottom diagram shows a line plot along the slab direction (Z axis) at a position indicated by the white dotted line. Note, that the line plot was generated from native images, rather than from MIP images, for better visualization.

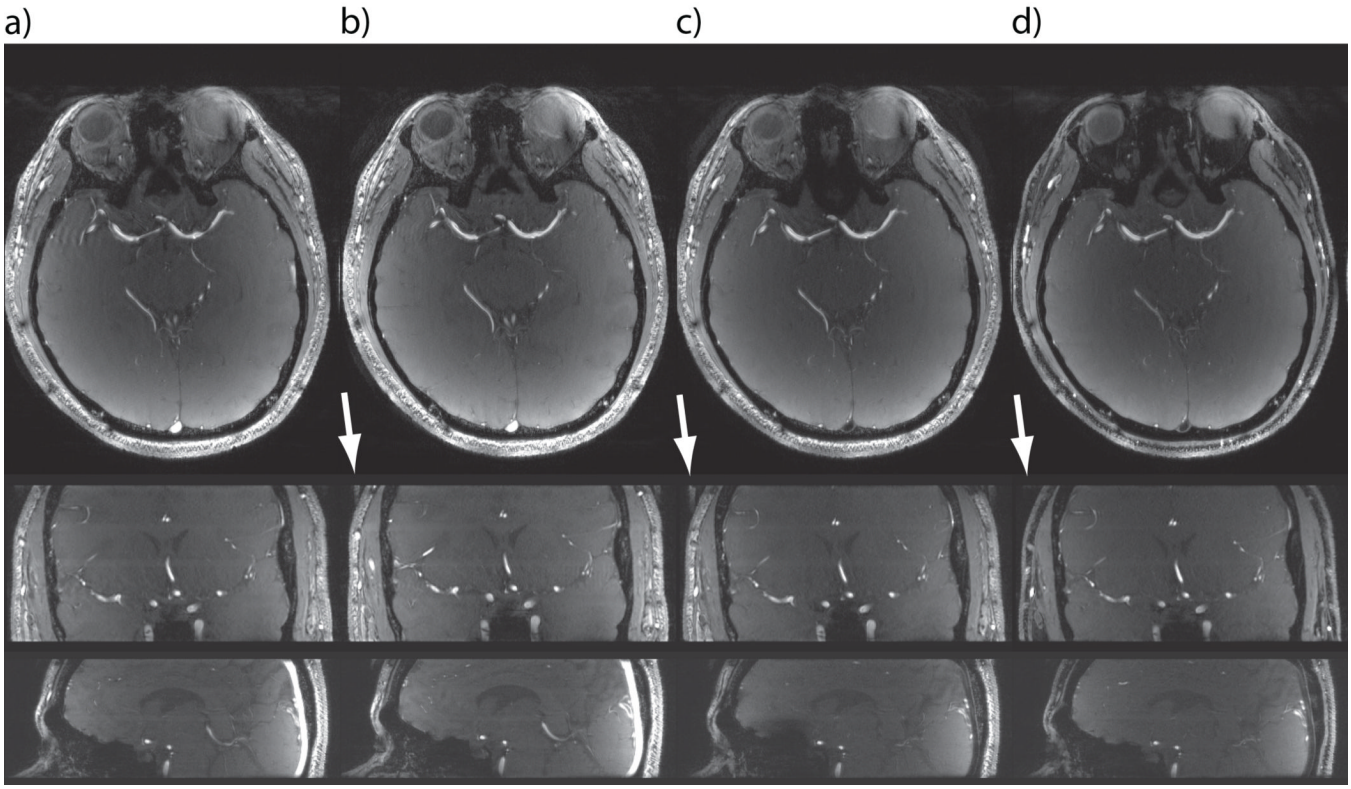

Figure 5.
Native TOF images acquired with (a) and without (b) applying VERSE on the excitation pulse, in the absence of venous saturation pulse. In (c) and (d) a VERSE saturation pulse (κ_{SAT}=25%) was used in addition to VERSE excitation. The polarity of the gradient (and correspondingly of the RF frequency) applied during the saturation pulse was reversed in (d) by comparison to (c).

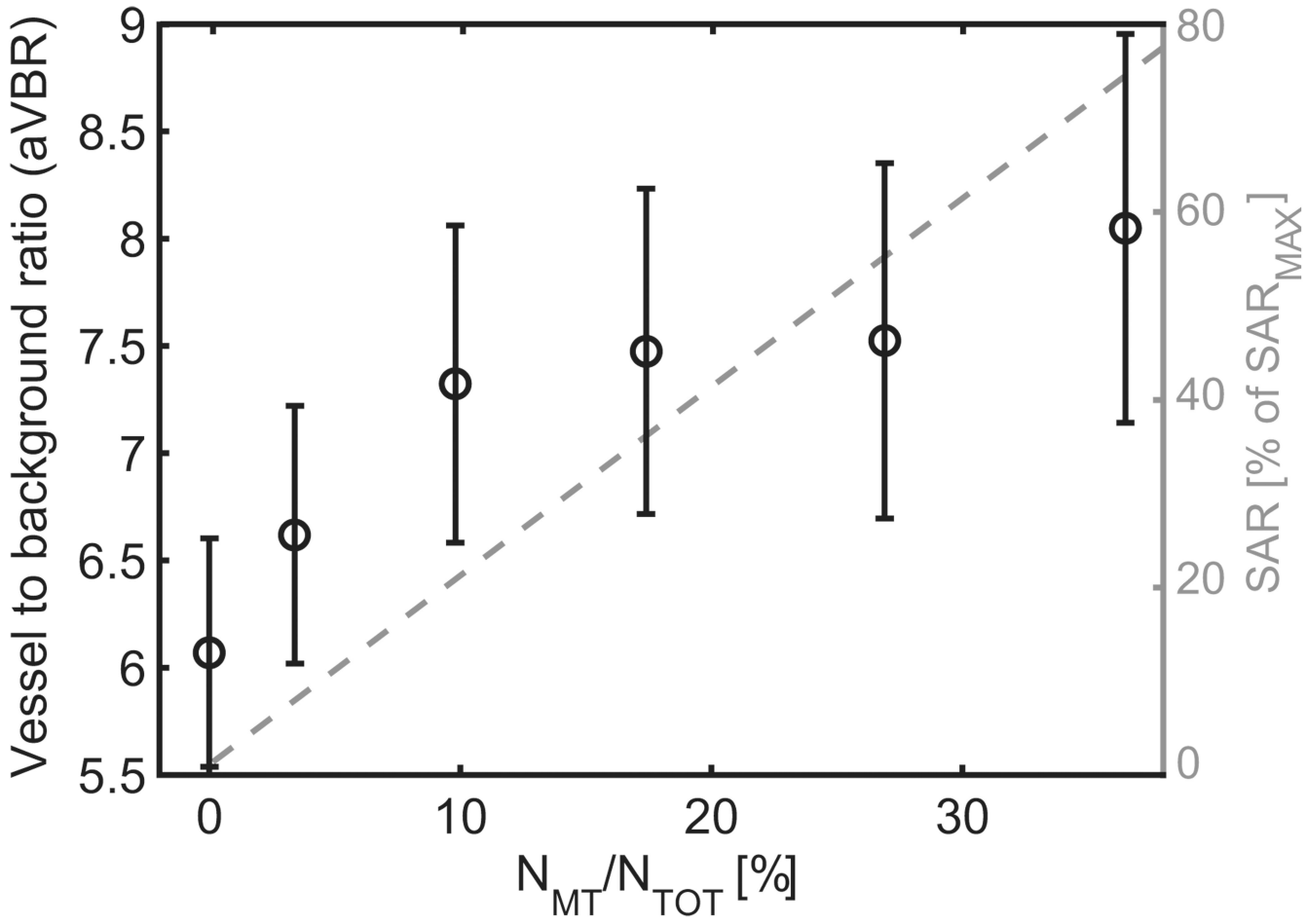

Figure 6.
Measured arterial vessel-to-background ratio (mean +/− error derived from standard deviation by error propagation through 5 subjects) and corresponding SAR (expressed in percent of SAR_{MAX}) generated by the MT pulses as a function of the number of MT pulses, given in percent of N_{TOT}.

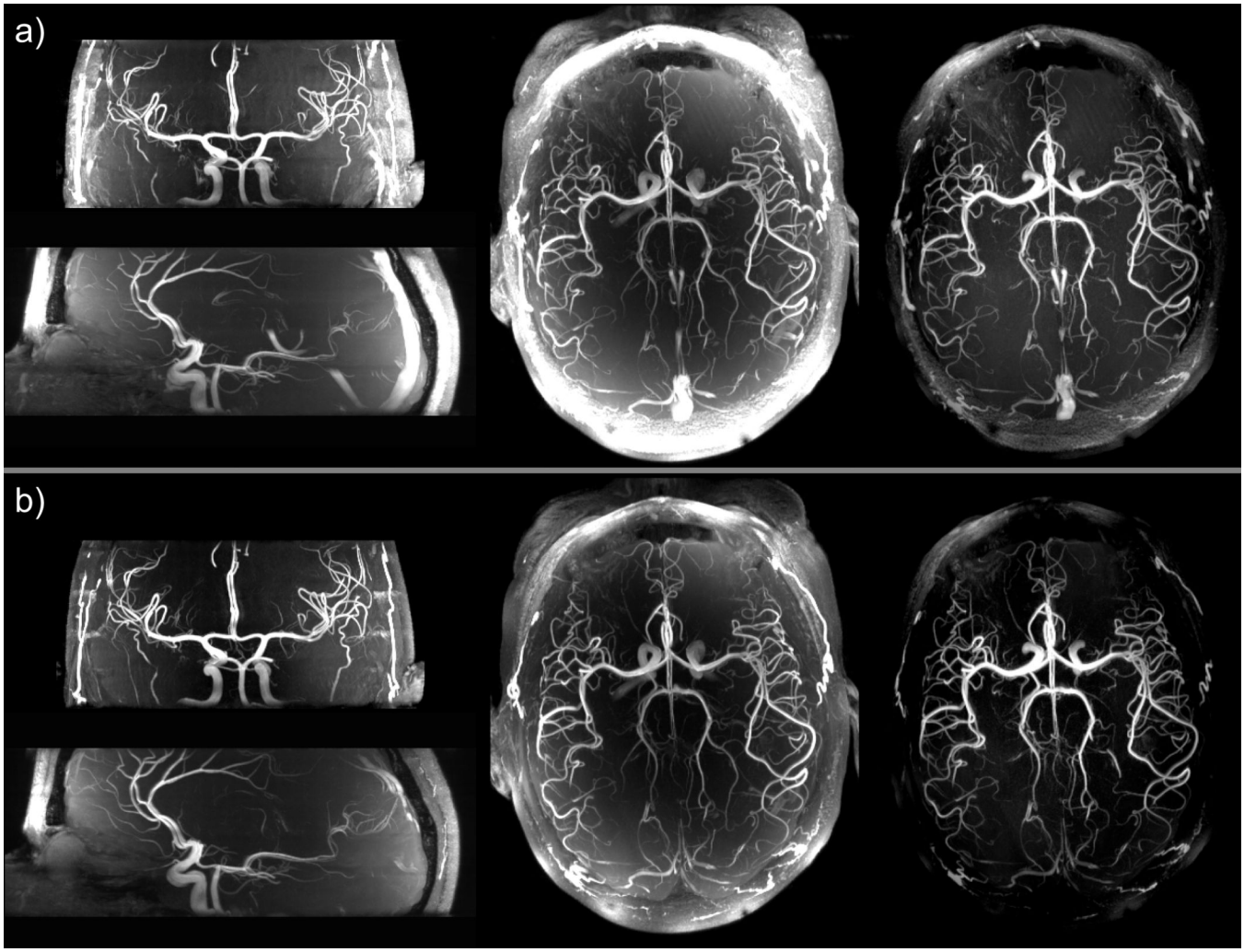

Figure 7.
Maximum intensity projection (MIP) images of multi-slab 3D TOF data sets acquired with: a) the initial TOF sequence without saturation pulse and without magnetization transfer pulses, and b) the modified TOF sequence using VERSE excitation, VERSE saturation and magnetization transfer pulses. The transversal MIP images are full projections through the 4 slabs, the sagittal and coronal MIP images are projections obtained over a 40 mm thickness. The corresponding imaging parameters are listed in Table 2. In the last column, transversal MIP images were obtained after correcting the acquired data for receive sensitivity induced signal variations. The product [B_1+ × proton density] was estimated by dividing smoothed small flip angle GRE images by the AFI map. A 2D polynomial fit of the latter ratio was then used to divide TOF data before generating the MIP images.

Table 1

Parameters for the excitation and saturation RF pulses and the corresponding selection gradients used in this study.

	Initial excitation pulse	**VERSE excitation pulse 1**	**VERSE excitation pulse 2**	**Initial saturation pulse**	**VERSE saturation pulse**
$b_{max}/\max[b_1(n)]^{\dagger}$	100%	50%	25%	100%	25%
Duration [μs]	1536	1536	1536	3584	3584
Slice thickness [mm]	24	24	24	40	40
G_{max} [mT/m]	6.04	6.76	11.61	1.28	2.35
G_{min} [mT/m]	-	3.02	1.51	-	0.32
pulse energy	100%	57.6%	33.9%	772%	296 %

†the ratio $\kappa=b_{max}/\max[b_1(n)]$ corresponds to κ_{EXC} and κ_{SAT} for excitation and saturation RF pulses, respectively. By our definition κ=100% when the VERSE algorithm is not applied.

Table 2

Imaging parameters for different acquisition modalities. Note that the set of imaging parameters in the rightmost column was used in multiple combinations of excitation, saturation and MT pulses, and with different levels of VERSE pulse design.

Sequence / **Parameters**	**Excitation profile in phantom**†	**Excitation profile in-vivo**†	**TOF in-vivo**
FOV x,y,z	160×160×72 mm^3	220×165×72 mm^3	220×172×78 mm^3
Resolution:	2.50×2.50×0.50 mm^3	3.43×3.43×1.00 mm^3	0.49×0.49×0.50 mm^3
Slab Thickness	24 mm	24 mm	24 mm
Slabs	1	1	4 (or 1‡)
TR / TE [ms]	80 ms / 2.8 ms	80 ms / 2.8 ms	33 ms / 3 ms
alpha (nominal)	20°	8°	24°
Slab oversampling	300%	300%	125%
Slab overlap	-	-	−25%
GRAPPA	1	1	3
Partial Fourier	-	6/8 (phase only)	6/8 (slab only)

† a modified 3D TOF sequence was used to measure the excitation profiles with larger imaging FOV along the slab axis

‡ only one slab was used when investigating the impact of applying VERSE on SAT pulses

Table 3

arterial vessel-to-background ratio (aVBR) and averaged SAR values determined by the scanner for the TOF (see Table 2, right column) using a reference voltage of 60 V. The aVBR calculated within two ROIs within/next to the basilar artery was averaged over 5 volunteers.

Excitation κ_{EXC}	Saturation κ_{SAT}	MT N_{MT}/N_{TOT}	SAR (% of SAR_{MAX})	aVBR
100%	100%	100%	319%	—
100%	100%	—	115%	—
100%	—	—	18%	6.3± 0.5
50%	—	—	11%	6.1 ± 0.5
50%	—	10%	31%	7.6 ± 0.7
50%	25%	—	49%	7.5 ± 0.8
50%	25%	10%	69%	9.4 ± 1.0